

3-D Printing Implementation of an X-band Eaton Lens for Beam Deflection

Guohong Du, *Member, IEEE*, Min Liang, *Student Member, IEEE*, Rafael Austrebert Sabory-Garcia, Changjun Liu, *Senior Member, IEEE*, and Hao Xin, *Senior Member, IEEE*

Abstract—In this letter, a 3-D Eaton lens with gradient refractive index (GRIN) distribution for beam deflection at X-band is designed, fabricated, and measured. The ideal 90° beam bending of Eaton lens is verified by the numerical simulation with the commercial software COMSOL Multiphysics. The practical refractive index of the lens is realized by controlling the mixing ratio of a polymer to air void. The dimensions of unit cell are designed with effective medium theory and verified by the full-wave simulation software ANSYS HFSS. A polymer jetting 3-D printing method is applied to implement the Eaton lens. The radiation pattern and near-field distribution of the lens are measured using an X-band waveguide as the feed, and the experimental results agree well with the simulated results.

Index Terms—3-D printing, beam deflection, Eaton lens, gradient refractive index (GRIN).

I. INTRODUCTION

EATON lenses, like Luneburg lenses and Maxwell's fish-eye lenses, are inhomogeneous dielectric lenses of which the refractive index distributions are functions of position and are often referred to as gradient refractive index (GRIN) devices. They have some unique and interesting characteristics that can be utilized in the design of antennas and radar targets. Eaton lenses are traditionally designed using geometrical theory of optics, i.e., Fermat's principle [1]. Most previous studies on Eaton lenses mainly focus on its electromagnetic property through theoretical analysis and numerical computation [2]. However, few of them have been realized in practice because of the inhomogeneous layered models. Recently, several variants of Eaton lens have been implemented using metamaterials design concept [3]. An inside-out Eaton lens has been made of H-fractal metamaterials for imaging application in a narrow band of frequencies [4]. These metamaterials-based designs consisted of copper-printed patterns on printed circuit boards (PCBs) as unit cell. In addition, a 2-D plasmonic Eaton lens

Manuscript received September 12, 2015; revised December 06, 2015; accepted December 22, 2015. Date of publication January 01, 2016; date of current version May 12, 2016. This work was supported in part by the AFOSR under Grant No. FA9550-13-1-0209, the National Science Foundation under Grant No. 0925220, the Program for Scientific Research Talent in CUIT under Grant No. J201403 and the 973 Program under Grant No. 2013CB328902.

G. Du is with the School of Electronics Engineering, Chengdu University of Information Technology, Chengdu 610225, China.

C. Liu is with the School of Electronics and Information Engineering, Sichuan University, Chengdu 610064, China.

M. Liang, R. A. Sabory-Garcia, and H. Xin are with the Electrical and Computer Engineering Department, University of Arizona, Tucson, AZ 85721 USA (e-mail: hxin@ece.arizona.edu).

Color versions of one or more of the figures in this letter are available online at <http://ieeexplore.ieee.org>.

Digital Object Identifier 10.1109/LAWP.2015.2514181

with 30 μm radius has been designed and experimentally realized with the truncated index profile [5].

In this letter, a 3-D all-dielectric Eaton lens is designed, fabricated, and characterized for beam deflection at X-band. X-band is chosen because it is a commonly used frequency range for a number of applications and fits quite well with the 3-D printer used in this work in terms of both unit cell size and aperture size. The 90° beam bending effectiveness of the lens with a 120-mm diameter ($4\lambda_0$ at 10 GHz) is demonstrated. The gradient refractive index distribution of the lens is realized by changing the filling ratio of polymer and air void locally at the unit cell level. The lens is fabricated using a polymer jetting 3-D printing technique. The near-field distribution and the far-field radiation pattern are both measured. The bent angles are measured at different feeding positions at X-band, and a 13-dB gain is observed when the bent angle is 37° at 10 GHz. The measured and simulated results agree well with each other.

II. EATON LENS DESIGN

A. Ideal Eaton lens

The index distribution of an ideal Eaton lens that bends light 90° satisfies [6]

$$n^2 = \frac{R}{nr} + \sqrt{\left(\frac{R}{nr}\right)^2 - 1} \quad (1)$$

where R is the radius of the lens and r is the distance from a point to the center of the sphere. Fig. 1 shows the refractive index and permittivity (ignoring loss) as a function of the distance r ranging from 0 to 60 mm for $R = 60$ mm (the diameter of 120 mm, $4\lambda_0$ at 10 GHz).

For the ideal Eaton lens, the refractive index quickly diverges as approaching the center of the lens. The characteristics of a 2-D Eaton lens with $R = 60$ mm at 10 GHz is simulated by the finite-element electromagnetic (EM) solver COMSOL as shown in Fig. 2. This lens consists of 12 layers at the interval of 5 mm, and the permittivity values range gradually from 1 for the outermost layer up to 11.6 for the innermost layer at the center. With a Gaussian beam incident upon the lens, a 90° beam deflection is apparent. The offset of the Gaussian source is 45 mm.

B. Eaton Lens Design Based on All-Dielectric Effective Media

Typical metamaterial designs tend to have narrow bandwidth and significant loss due to the use of resonant metallic unit cell.

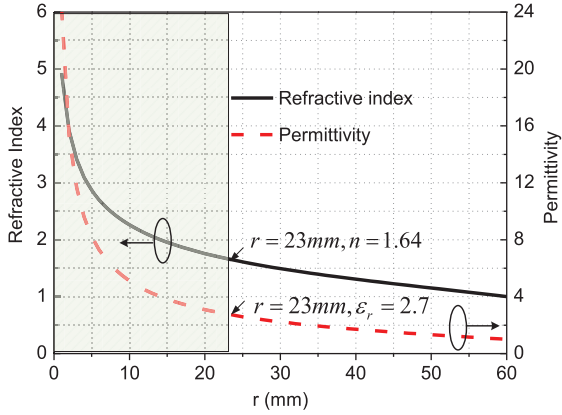


Fig. 1. Spatial distribution of refractive index and permittivity for an Eaton lens with a 120-mm diameter ($R = 60$ mm) versus r .

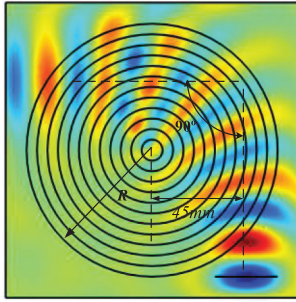


Fig. 2. Electric field distribution of a 2-D Eaton lens ($R = 60$ mm) simulated at 10 GHz using COMSOL.

To overcome this problem, an all-dielectric effective medium approach is utilized here. An Eaton lens is designed to be composed of discrete polymer cubes ($\epsilon_r = 2.7$, $\tan\delta = 0.02$) with thin polymer rods as connectors/supporters for the whole structure. The effect of these thin rods on the electromagnetic property of the lens can be neglected since they have very small dimensions compared to unit cell size. The effective permittivity of the unit cells is controlled by the filling ratio of polymer to air void based on the effective medium theory.

The designed Eaton lens has a diameter of 112.3 mm (about $4\lambda_0$ at 10 GHz) and a cubic unit cell size of 5 mm, which is $1/6$ of the wavelength in free space at 10 GHz, as shown in Fig. 3. Because the exact effective permittivity in practice is a little different from that calculated by the ideal effective medium theory, full-wave finite-element software ANSYS HFSS is also used to numerically extract the effective permittivity of unit cells from the simulated S -parameters [7]. To obtain the required box size for any desired permittivity, an exponential fit of the effective permittivity as a function of the unit cell geometry is applied as shown in Fig. 3. The fitted function [8] is

$$b = 5.5593 - 590974e^{-\epsilon_r/0.07958} - 9.54823e^{-\epsilon_r/0.95537} \quad (2)$$

where b is the box size and ϵ_r is the expected permittivity. Since the maximum achievable effective permittivity is 2.7 when the polymer filling ratio is 100% of the unit cell, the permittivity distribution in (1) is truncated with limited range from 1 for the outermost layer up to 2.7 in the center as shown in Fig. 1.

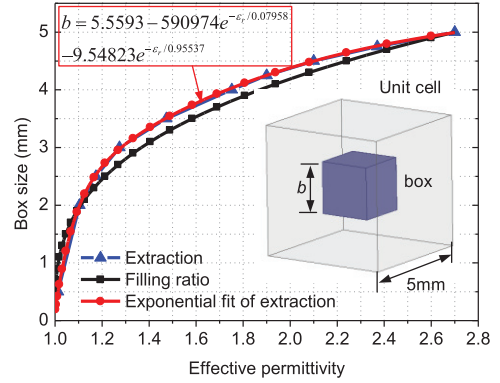


Fig. 3. Effective permittivity of unit cell with different box sizes [8].

C. HFSS Simulation of Designed Eaton Lens

The whole 3-D model of Eaton lens consists of 5725 unit cells with different box sizes and a solid sphere in the center region with a radius of 23 mm as shown in Fig. 4(a). In Fig. 4(b), an X-band waveguide WR-90 with the inside dimensions 22.86×10.16 mm² is placed in the horizontal (xy) plane as TE wave excitation with the electric field in the z -direction. In order to reduce the simulation time, the flange of the open-ended waveguide is simplified. There is a shifted distance of $d = 32$ mm from the center of waveguide aperture to the y -axis. Fig. 4(c) shows the simulated radiation pattern in the xy -plane compared to measured results that will be discussed in Section III. It is observed that the simulated gain of the Eaton lens is 13.8 dB at -34° , while the gain of the waveguide without lens is 7.8 dB. Based on Fermat's principle, the gradient index distribution of the lens changes the phase velocity of the incident wave nonuniformly and effectively distributes the incident wave over a larger aperture while maintaining the planar wavefront of the incident wave. Therefore, the Eaton lens enhances the radiation gain.

However, due to the truncated index distribution in the central part of the lens, the simulated beam bent angle of the 3-D Eaton lens is 34° instead of 90° as in Fig. 2. Other possible reasons that induce this 90° to 34° bending angle difference include the unit cell discretization of the continuous gradient refractive index and the nonideal incident wave using open-ended waveguide.

III. FABRICATION AND MEASUREMENT

A. Fabrication by Polymer Jetting 3-D Printing

The Eaton lens is printed using a polymer jetting rapid prototyping technique that allows fast and inexpensive fabrication of polymer components with arbitrary shapes and complexity. A commercial rapid prototyping machine Objet Eden 350 is employed here. First of all, the designed 3-D structure of Eaton lens is exported from HFSS into an STL file to obtain a series of model slices for the printer. After each slice, which is composed of the model polymer material and water-soluble support materials, printed, a high-pressure water spray is used to wash away the support material while leaving the model

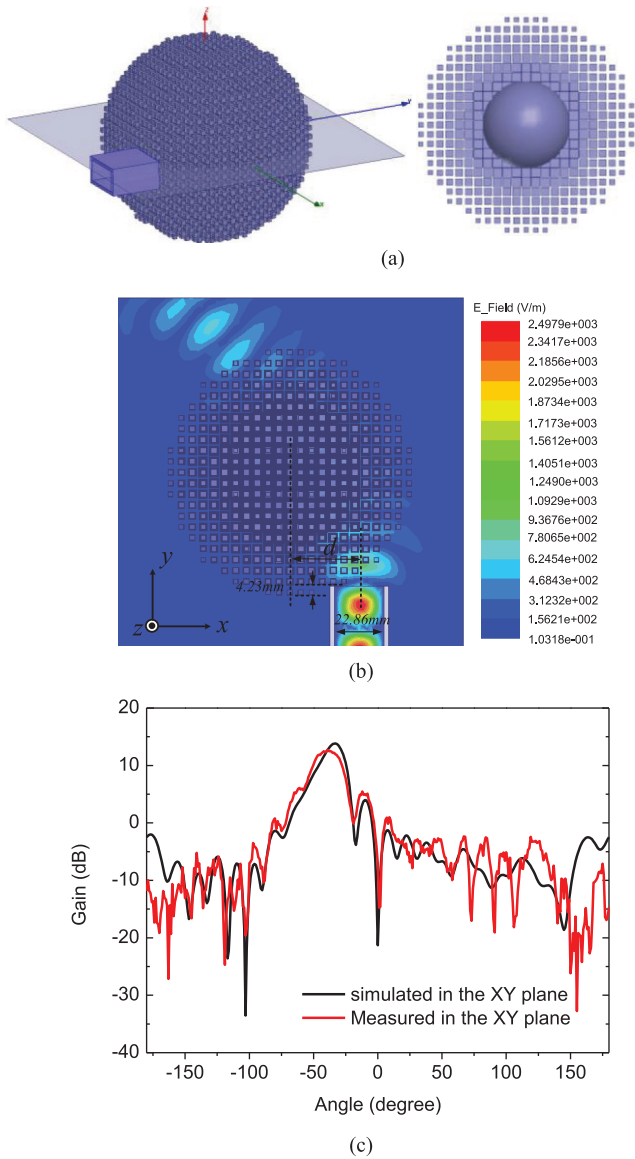


Fig. 4. Simulated property of the 3-D Eaton lens with truncated index distribution using HFSS. (a) 3-D Eaton lens HFSS model and its cross section. (b) Near-field electric field distribution of the lens. (c) Far-field radiated pattern of the lens compared with measurement results.

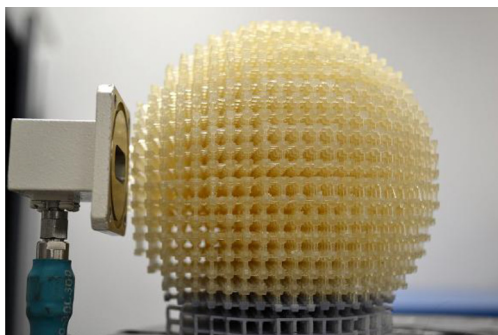


Fig. 5. Photograph of the Eaton lens.

material intact. Then, the whole lens is assembled from all the printed layers. A photograph of the final Eaton lens is shown in Fig. 5.

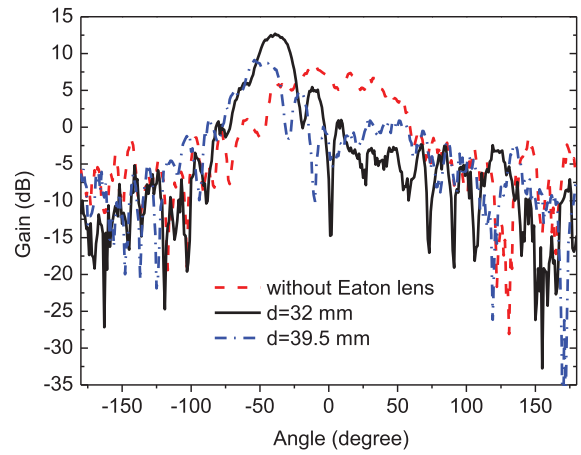


Fig. 6. Measured radiation pattern of Eaton lens.

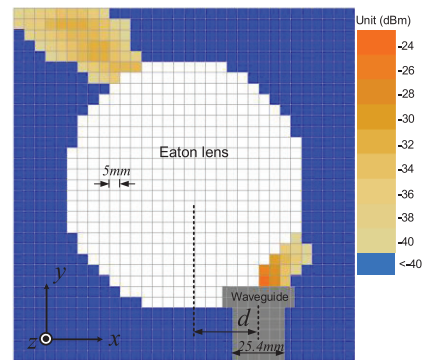


Fig. 7. Measured near-field distribution of the Eaton lens ($d = 32$ mm).

B. Measurement of the Fabricated Eaton Lens

To characterize the fabricated Eaton lens, an experiment platform as shown in Fig. 5 is set up. An X-band waveguide WR-90 with the outside dimensions $25.4 \times 12.7 \text{ mm}^2$ is used to feed the lens. The far-field radiation pattern is measured by a vector network analyzer HP-8720C. A pair of standard gain horn antennas is used to calibrate the gain of the lens. The measured far field patterns in the horizontal (xy) plane at 10 GHz for two waveguide feeding locations as well as a reference pattern without the lens are plotted in Fig. 6. The red dashed line represents the waveguide aperture gain measured without the Eaton lens, which has a wide main lobe. When the waveguide aperture is placed the same way as shown in Fig. 4(b) with $d = 32$ mm, a 37° beam bending is obtained with a gain of 13 dB (solid black line), which agrees reasonably well with the simulated results in Fig. 4(c). The half-power beamwidth is 23° . When the waveguide is moved from $d = 32$ mm to 39.5 mm, the flange maintains the same height, and the bent angle is increased to 49° (blue dotted line). However, a smaller gain of 9 dB is observed because only a part of the power from the waveguide aperture enters the lens.

The measured input reflection coefficient of the waveguide with the Eaton lens is -13 dB. The permittivity value of the lens gradually changes from 1 for the outermost layer to the 2.7 for the central solid sphere. Thus, the outermost layer is matched to the free space.

The near-field distribution of the Eaton lens in the horizontal plane is also measured at 10 GHz. An analog signal generator Agilent-E8257 C and a spectrum analyzer Agilent-E4407B are used as the transmitter and receiver, respectively. The generator output power to the waveguide feed is 20 dBm. A coaxial probe is scanned in two dimensions (x and y) in the horizontal plane with 5-mm steps in both directions. The measured near-field distribution plotted in Fig. 7 further validates the Eaton lens design.

IV. CONCLUSION

An all-dielectric Eaton lens is designed and fabricated using a 3-D printer based on polymer jetting technique for beam deflection. The electromagnetic properties of the printed lens are characterized. Both the measured and simulated far-field radiation pattern and near-field distribution of the Eaton lens demonstrate the capability of wave deflection. The bent angle is 37° with 13 dB gain at 10 GHz.

REFERENCES

- [1] A. D. Greenwood and J. Jin, "A filed picture of wave propagation in inhomogeneous dielectric lenses," *IEEE Antennas Propag. Mag.*, vol. 41, no. 5, pp. 9–18, Oct. 1999.
- [2] A. Akbarzadeh and A. J. Danner, "Generalization of ray tracing in a linear inhomogeneous anisotropic medium: A coordinate-free approach," *J. Opt. Soc.*, vol. 27, no. 12, pp. 2558–2562, Dec. 2010.
- [3] T. M. Chang, G. Dupont, S. Enoch, and S. Guenneau, "Enhanced control of light and sound trajectories with three-dimensional gradient index lenses," *New J. Phys.*, vol. 14, p. 035011, 2012.
- [4] Q. Wu *et al.*, "An inside-out Eaton lens made of H-fractal metamaterials," *Appl. Phys. Lett.*, vol. 101, p. 031903, 2012.
- [5] T. Zentgraf, Y. Liu, M. H. Mikkelsen, J. Valentine, and X. Zhang, "Plasmonic Luneburg and Eaton lenses," *Nature Nanotechnol.*, vol. 6, pp. 151–155, 2011.
- [6] A. J. Danner and U. Leonhardt, "Lossless design of an Eaton lens and invisible sphere by transformation optics with no bandwidth limitation," *Proc. CLEO*, Baltimore, MD, USA, 2009.
- [7] D. R. Smith, D. C. Vier, T. Koschny, and C. M. Soukoulis, "Electromagnetic parameter retrieval from inhomogeneous metamaterials," *Phys. Rev. E*, vol. 71, p. 036617, 2005.
- [8] M. Liang *et al.*, "A 3-D Luneburg lens antenna fabricated by polymer jetting rapid prototyping," *IEEE Trans. Antennas Propag.*, vol. 62, no. 4, pp. 1799–1807, Apr. 2014.